Optics Letters

Remote and rapid micromachining of broadband low-reflectivity black silicon surfaces by femtosecond laser filaments

Xuepeng Zhan,[1] Huailiang Xu,[1,*] Chunhao Li,[1] Hongwei Zang,[1] Chang Liu,[1] Jihong Zhao,[1] and Hongbo Sun[1,2]

[1]State Key Laboratory on Integrated Optoelectronics, College of Electronic Science and Engineering, Jilin University, Changchun 130012, China
[2]College of Physics, Jilin University, Changchun 130012, China
*Corresponding author: huailiang@jlu.edu.cn

Received 30 November 2016; revised 23 December 2016; accepted 23 December 2016; posted 3 January 2017 (Doc. ID 281807); published 25 January 2017

We report an approach for remote and rapid fabrication of a broadband low-reflectivity black silicon surface by ablating crystalline silicon with femtosecond laser filaments in air. Porous microstructures on the processed silicon surface are formed, resulting in a significantly enhanced light trapping efficiency in a broadband (UV-IR) spectral range. It is found that the air filament can significantly reduce the average number of adopted pulses in a normalized fabrication area and enables the processing remotely, which opens a way toward remote and rapid micromachining of optoelectronic materials by femtosecond laser filaments. © 2017 Optical Society of America

OCIS codes: (140.3390) Laser materials processing; (220.4000) Microstructure fabrication; (190.4350) Nonlinear optics at surfaces.

https://doi.org/10.1364/OL.42.000510

Silicon has been considered to be the most fundamental material in optoelectronic devices such as solar cells and photovoltaic sensors [1,2]. However, light absorptive efficiency of silicon that plays a decisive role in the sensitivity and quality of these optoelectronic devices is relatively low, owing to the high reflection resulting from the intrinsic refractive index mismatch of air and silicon [3]. Therefore, a variety of methods have been developed to improve the light absorptive efficiency of silicon, and it was shown that micro/nano-scale structures formed on silicon surface can efficiently decrease the reflectivity of the silicon [4,5], giving rise to a broadband ultralow reflectivity silicon surface, popularly called "black silicon" [6].

Among the techniques available for producing black silicon, femtosecond laser processing has proved to be very reliable for precisely fabricating the designed micro/nano-scale structures on a silicon surface with ultrahigh spatial resolution far beyond the optical diffraction limit [7–9]. Nevertheless, the reported black silicon fabricated by femtosecond laser processing is all from near-field experiments, which require the laser beam to be tightly focused on the sample, leading unavoidably to some limitations. As the micromachining resolution is as high as several micrometers, it is time-consuming to achieve a large-scale fabrication area. Moreover, owing to the tight convergence of the femtosecond laser beam, planar samples with ultra-smooth surface are required, which brings extreme difficulties to meeting the demand of the fabricating microstructures on curved surfaces, especially irregular ones. Therefore, it is becoming a challenge to develop a rapid and far-field microstructure processing technique that enables large-scale fabrication of untreated silicon samples.

Recently, femtosecond laser filament has been utilized in the field of remotely cutting and drilling metals and biological materials such as flesh and bones [10]. Filamentation results from a dynamics competition between the nonlinear optical Kerr self-focusing and defocusing of the self-generated plasma [11], leading to nearly constant intensity of $\sim 10^{13}$–10^{14} W/cm^2 in a long (from a few centimeters up to tens of meters) plasma channel with a diameter of ~100–200 μm. Attractive properties of the light filament in terms of remote delivery of high laser intensity, supercontinuum generation, and electric conductivity have provided a lot of applications in the fields of lighting control, THz generation, and remote sensing [11–13].

In this Letter, we experimentally demonstrate the formation of microscale porous structures on silicon surfaces by remotely ablating crystalline silicon with femtosecond laser filaments. It is found that the filament-induced ablation of crystalline silicon changes the surface topography and chemical composition of the crystalline silicon with amorphous silicon formed in the processed region. The porous microstructures on the silicon surface give rise to a significantly enhanced light trapping efficiency with a reduced average number of adopted pulses in a normalized fabrication area, showing the ability of remote and rapid micromachining of broadband low-reflectivity black silicon surfaces by femtosecond laser filament.

The experiments were carried out using a Ti:sapphire femtosecond laser amplifier (Spectra-Physics) with a central wavelength of 800 nm, a pulse duration of 35 fs, and a repetition rate of 500 Hz. Unlike complex and compact near-field fabrication

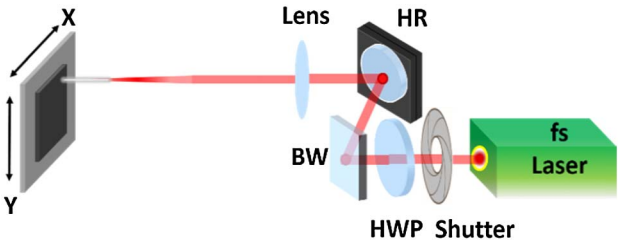

Fig. 1. Schematic diagram of the experimental setup for the femtosecond laser processing system. HWP, half-wave plate; BW, Brewster window; HR, high-reflective lens.

systems, the femtosecond filament processing system we developed is relatively simple. As presented by the experimental setup in Fig. 1, the linearly polarized laser pulses from the laser amplifier were focused by a 1 m lens to directly generate a single filament in air with a length of ~3 cm and a diameter of ~100–200 μm. An electrical shutter was inserted into the laser propagation path to control the laser shots on the sample. The laser energy was ~2 mJ, which was controlled by a half-wave plate and a Brewster window, and the beam diameter is ~1.0 cm with a Gaussian spatial profile.

A 250 μm thick *N*-type crystalline Si (100) wafer with the area of 20 × 20 mm was mounted on a platform equipped on a 2D translation stage (horizontal and vertical directions) with a step resolution of 2.5 μm. The silicon wafer was placed at a right angle to the laser filament propagation direction, and was about 1 m away from the focal lens. Before the fabrication, the crystalline silicon wafer was cleaned by acetone, ethanol, and deionized water. In the raster scan, the silicon wafer sample was totally processed via continuously moving the 2D motorized stage, which allowed precise positioning of the light filament on the surface silicon.

After the interaction of the femtosecond laser filament with the silicon wafer, the topography of surface structural modifications on silicon was measured using a field emission scanning electron microscope (SEM, JEOL JSM-7500F). A comparative examination of elemental compositions of both unprocessed and processed silicon samples was performed using an energy dispersive spectrometer (EDS, EDAX AMETEK). The absorption spectra of the silicon wafers in the spectral range of 200–2500 nm were characterized by a spectrophotometer UV-3600 (Shimadzu Company) equipped with an integrating sphere (LISR-UV). In order to analyze the crystal orientation of the silicon, a Raman spectrometer (LabRAM HR Evolution, Horiba Scientific) with a 532 nm laser as the excitation source was used to measure the Raman spectrum of the silicon sample.

Figure 2 shows the top-view SEM images of the processed silicon surface morphology with the scanning speeds of Fig. 2(a) 20 mm/s, Fig. 2(b) 15 mm/s, Fig. 2(c) 10 mm/s, and Fig. 2(d) 5 mm/s, respectively. The insets (I) in Fig. 2 are the SEM images in a higher resolution. It can be clearly seen from Fig. 2 that for all the scanning speeds femtosecond laser filaments can modify the silicon surface, resulting in micro-scale porous structures. Although the processing resolution is limited by the large filament diameter (~100 μm in air [11]), sub-10 micrometer, and even nanometer, structures could be fabricated on the silicon surface. It can be noted that the average size of the porous microstructures becomes larger, from ~5 to ~15 μm as the line

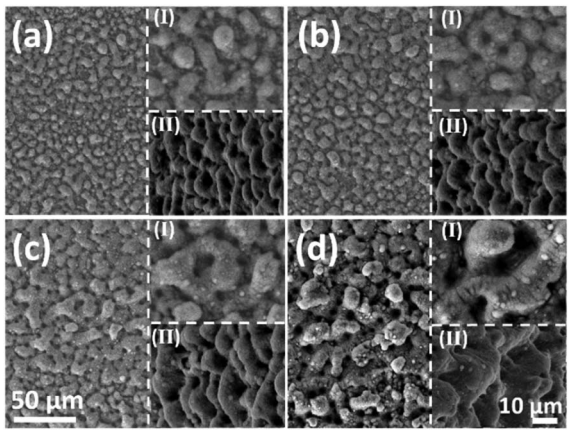

Fig. 2. Top-view SEM images for the processed silicon samples with different line scanning speeds of (a) 20 mm/s, (b) 15 mm/s, (c) 10 mm/s, and (d) 5 mm/s. Insets: (I) top- and (II) tilt-view SEM images in a higher resolution.

scanning speed decreases from 20 to 5 mm/s, which originates from a different number of the pulses being applied to the silicon wafer. According to the repetition rate of 500 Hz and the size of the filament is about 100 μm, it is estimated that each spot on the silicon sample in one scan would be hit, for example, by five pulses with the scanning speed of 10 mm/s. It can also be observed from the higher resolution SEM images shown in the insets of Fig. 2 that the depth of the textured pattern on the silicon surface changes as a function of the line scanning speed. To show the details of the depth changes, 45 deg tilt-view SEM images of the silicon surface morphology were measured, as shown in the insets (II) of Fig. 2, from which the depths of the micro-hole structures are determined to be about 14, 12, 8, and 6 μm for the scanning speeds of Fig. 2(d) 5 mm/s, Fig. 2(c) 10 mm/s, Fig. 2(b) 15 mm/s, and Fig. 2(a) 20 mm/s, respectively.

It can also be seen from the insets of Fig. 2 that there are some micro/nano-particles deposited randomly on the microstructures, which might be caused by the fusion of the silicon heated by the ultrahigh peak pulses [6]. Since the fusion could stimulate the chemical reaction of the silicon and air molecules, the chemical compositions of these micro/nano structures are examined by EDS, as shown in Fig. 3, from which the elements of oxygen and silicon are detected, and the mass fraction of oxygen is increased when compared with the unprocessed silicon sample, indicating the formation of SiO_x compounds on the silicon surface.

The structural properties of the fabricated silicon surface are further examined by Raman spectroscopy. Figure 4 shows the Raman spectra for Fig. 4(a), the unprocessed silicon sample, and the fabricated samples with different scanning speeds of Fig. 4(b) 25 mm/s, Fig. 4(c) 20 mm/s, Fig. 4(d) 15 mm/s, Fig. 4(e) 10 mm/s, and Fig. 4(f) 5 mm/s. It can be seen that all the samples show a strong vibration peak at 520 cm^{-1}, which can be assigned to the Si-I structure, coming from the original diamond structure of crystalline silicon. It can be noted that line width of the 520 cm^{-1} peak is broadened for the processed samples, indicating the existence of residual tensile stress [14,15]. Besides the 520 cm^{-1} peak, a new broad peak at around 480–490 cm^{-1} emerges and becomes stronger as the

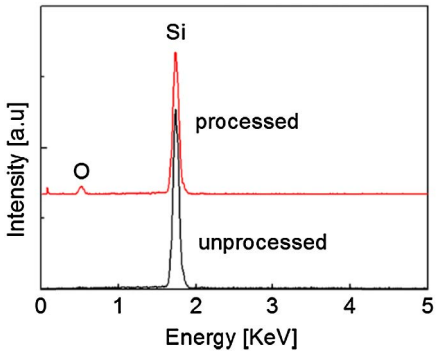

Fig. 3. EDS results for the (top) processed and (bottom) unprocessed silicon samples.

line scanning speed decreases from 25 to 5 mm/s. This peak is assigned to amorphous silicon (α-Si). The observation of amorphous silicon clearly indicates that femtosecond laser filaments can induce the fusion of the crystalline silicon and destroy the crystal orientation. The stronger peaks for the slower scanning speed means that a larger amount of amorphous silicon can be produced by increasing the number of the pulses applied on the silicon. The above results clearly show that the high intensity inside the filament plays a crucial role in the formation of microstructures on the silicon surface. It should be pointed out that no peaks belonging to SiO_x could be observed in the Raman spectra, implying that the amount of the produced SiO_x compounds on the silicon surface could be very low.

In order to check the light trapping ability of the processed silicon, the silicon wafers were fabricated by scanning the wafer horizontally back and forth with the wafer shifted vertically after each horizontal scanning turn. Figure 5 shows the SEM images of the fabricated silicon wafer with the horizontal scanning speeds of Figs. 5(a)–5(c) 10 mm/s and Figs. 5(d)–5(f) 5 mm/s and the vertical distance intervals of Figs. 5(a) and 5(d) 300 μm, Figs. 5(b) and 5(e) 200 μm, and Figs. 5(c) and 5(f) 100 μm, respectively. It can be seen from Fig. 5 that the micro-structured lines produced by femtosecond filaments have a width of about ~150 μm, corresponding to the filament diameter with nearly uniform intensity distribution. The adjacent microstructure lines for the intervals of Figs. 5(a) and 5(d)

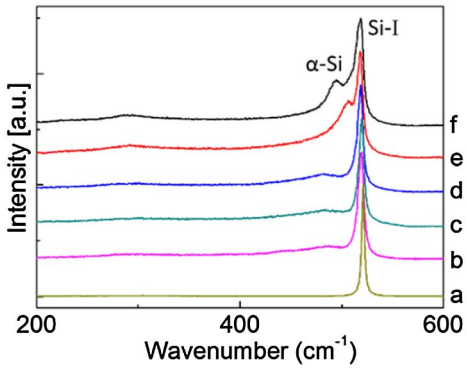

Fig. 4. Raman spectra measured for the (a) unprocessed and (b)–(f) processed silicon samples with different line scanning speeds of (b) 25 mm/s, (c) 20 mm/s, (d) 15 mm/s, (e) 10 mm/s, and (f) 5 mm/s.

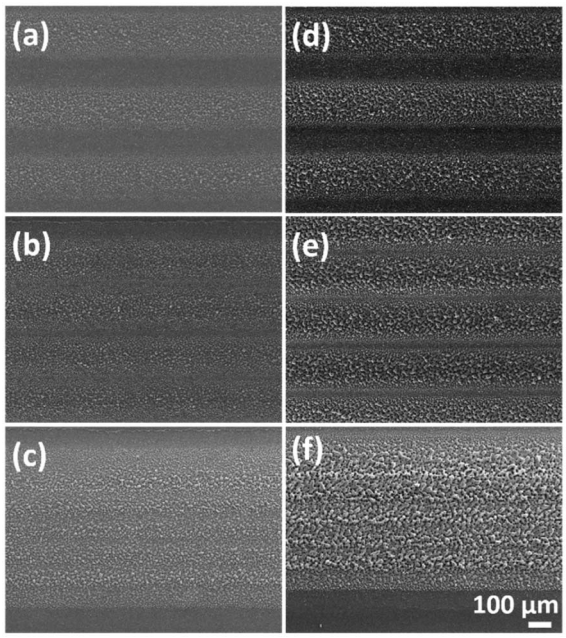

Fig. 5. Top-view SEM images of the processed silicon samples with different adjacent intervals of (a), (d) 300 μm; (b), (e) 200 μm; and (c), (f) 100 μm, and different line scanning speeds of (a)–(c) 10 mm/s and (d)–(f) 5 mm/s.

300 μm and Figs. 5(b) and 5(e) 200 μm are totally separated with a grating-like pattern, while those for the intervals of Figs. 5(c) and 5(f) 100 μm overlap, forming a pattern without obvious boundaries.

Figure 6(a) shows the absorption spectra of the silicon samples processed with a fixed scanning speed of 5 mm/s, but different line intervals of (dashed) 100, (solid) 200, and (dashed line) 300 μm, respectively. The absorption spectrum of the unprocessed silicon sample is also shown in Fig. 6 as a reference (dotted). It can be seen that the light trapping abilities of the processed silicon samples in a broad spectral range are significantly enhanced, with the absorbance of ~90–97% in the spectral range of ~0.2–1.1 μm, which decreases gradually from 1.1 to 2.5 μm, showing a similar behavior as those fabricated in air using near-field methods [16]. The light trapping ability is slightly better when there is no boundary between two adjacent lines (dashed line for the line interval of 100 μm). The similar absorption efficiencies imply that the unobvious micro/nano structures that result from the energy reservoir around the filament between the fabricated lines also make a contribution to the absorption. Similar results were also obtained with different line scanning speeds, as shown in Fig. 6(b).

The observed enhanced absorption can be explained as follows. It is well known that the underlying mechanism for the light absorption of the unprocessed (smooth and flat) silicon originates from band transitions, lattice vibration and the absorption due to free carriers, impurities or lattice defects. For the processed silicon, the produced porous micro/nanoscale structures play an important role in increasing the light trapping ability. For the spectral range in the above-band gap ($\lambda = 0.2$–1.1 μm), the surface structures that are smaller than an optical wavelength can contribute to light absorption due to an effective graded refractive index layer at the air/solid interface.

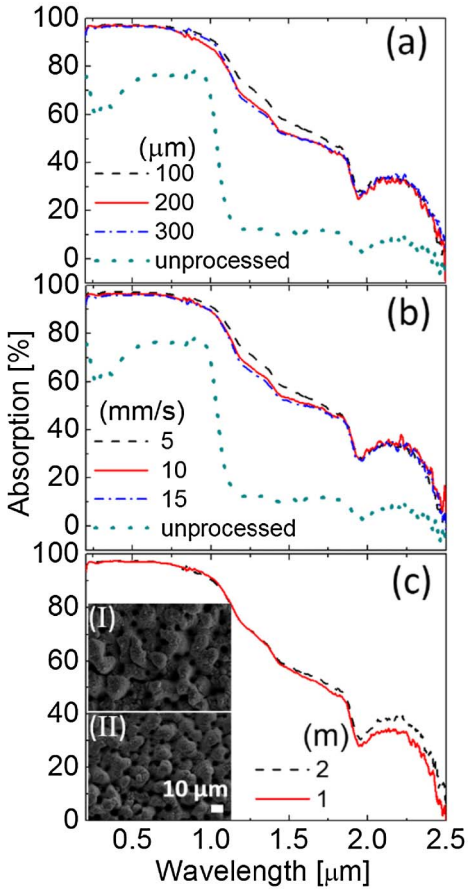

Fig. 6. Absorption spectra measured for the processed samples with different (a) scanning intervals at a fixed line scanning speed of 5 mm/s, (b) line scanning speeds at a fixed interval of 100 μm, and (c) focal lens at a fixed line scanning speed of 5 mm/s and an interval of 100 μm. The absorption spectrum of the unprocessed silicon is also shown in (a)–(c) for comparison. Insets: SEM images of the samples obtained with the focal lens of (I) f =1 m and (II) f = 2 m, respectively.

The structures larger than an optical wavelength can trap the light due to multiple reflections [4,17]. While for the spectral range in the below-band gap ($\lambda = 1.1$–2.5 μm), the enhanced absorption might be caused by structure defects introduced during femtosecond light bullet processing. According to the EDS result, the deposition of the elements such as Oxygen might lead to the defects in the deep energy level of silicon, increasing the absorption efficiency of silicon.

To further show the ability of remote processing of black silicon by femtosecond laser filament, we performed a 2 m fabrication experiment by generating a single filament in air by a 2 m focal lens. All other experimental conditions such as the laser energy and pulse duration were remained the same as before. The peak intensities inside the filament are estimated to 1.3×10^{14} W/cm^2 and 1.0×10^{14} W/cm^2 for 1 m (f-number = 100) and 2 m (f-number = 200) focal lens, respectively [18], which produced similar porous microstructures, as shown in the insets of Fig. 6(c). By measuring the absorption spectra [Fig. 6(c)], the processed sample at the 2 m distance (dashed) gives nearly the same broadband high absorption in the range of 0.2–2.5 μm as that obtained with the 1 m lens (solid), confirming the remote repeatability and stability of femtosecond laser filament processing.

In summary, we have demonstrated the feasibility for remote and rapid fabrication of black silicon by a femtosecond laser filament in air. The surface topography of porous microstructures was formed on the processed crystalline silicon, giving rise to significant light trapping enhancement of the silicon surface in a broadband spectral range from UV to IR, and the broadband high-absorption black silicon could be easily created at an extended distance. The Raman and EDS measurements indicated the changes of crystalline orientation and chemical compositions in the processed region. Due to the intrinsic ability of the femtosecond laser filament in remotely delivering ultrahigh laser intensity, our results show the potential of femtosecond filament processing in remote and rapid micromachining of optoelectronics materials.

Funding. National Natural Science Foundation of China (NSFC) (61625501, 61235003, 61427816); National Basic Research Program of China (2014CB921300); Open Fund of the State Key Laboratory of High Field Laser Physics (SIOM)

REFERENCES

1. J. E. Carey, C. H. Crouch, M. Shen, and E. Mazur, Opt. Lett. **30**, 1773 (2005).
2. L. Alloatti, R. Palmer, S. Diebold, K. P. Paul, B. Chen, R. Dinu, and C. Koos, Light Sci. Appl. **3**, e173 (2014).
3. A. Y. Vorobyev and C. Guo, Appl. Surf. Sci. **257**, 7291 (2011).
4. H. M. Branz, V. E. Yost, S. Ward, K. M. Jones, B. To, and P. Stradins, Appl. Phys. Lett. **94**, 231121 (2009).
5. L. L. Ma, Y. C. Zhou, N. Jiang, X. Lu, J. Shao, W. Lu, and X. Y. Hou, Appl. Phys. Lett. **88**, 171907 (2006).
6. T. H. Her, R. J. Finlay, C. Wu, S. Deliwala, and E. Mazur, Appl. Phys. Lett. **73**, 1673 (1998).
7. C. H. Li, J. H. Zhao, Q. D. Chen, J. Feng, W. T. Zheng, and H.-B. Sun, IEEE Photon. Technol. Lett. **27**, 1481 (2015).
8. J. Yang, F. Luo, T. S. Kao, X. Li, G. W. Ho, J. Teng, and M. Hong, Light: Sci. Appl. **3**, e185 (2014).
9. M. A. Sheehy, L. Winston, J. E. Carey, C. M. Friend, and E. Mazur, Chem. Mater. **17**, 3582 (2005).
10. D. Kiselev, L. Woeste, and J. P. Wolf, Appl. Phys. B **100**, 515 (2010).
11. S. L. Chin, *Femtosecond Laser Filamentation* (Springer, 2010).
12. J. Kasparian, M. Rodriguex, G. Mejean, J. Yu, E. Salmon, H. While, R. Bourayou, S. Frey, Y. B. André, A. Mysyrowicz, R. Sauerbrey, J. P. Wolf, and L. Wöste, Science **301**, 61 (2003).
13. H. L. Xu, Y. Cheng, S. L. Chin, and H. B. Sun, Laser Photon. Rev. **9**, 275 (2015).
14. Y. Gogotsi, C. Baek, and F. Kirscht, Semicond. Sci. Tech. **14**, 936 (1999).
15. A. Kailer, Y. G. Gogotsi, and K. G. Nickel, J. Appl. Phys. **81**, 3057 (1997).
16. R. Younkin, J. E. Carey, E. Mazur, J. A. Levinson, and C. M. Friend, J. Appl. Phys. **93**, 2626 (2003).
17. C. H. Crouch, J. E. Carey, M. Shen, E. Mazur, and F. Y. Genin, Appl. Phys. A **79**, 1635 (2004).
18. X. L. Liu, W. B. Cheng, M. Petrarca, and P. Polynkin, Opt. Lett. **41**, 4751 (2016).